



The Pulsed Periodic Discharge in Mixtures of Ar with Sulfur Vapour

S. V. Avtaeva¹ · A. A. Heneral²

Received: 26 July 2019 / Accepted: 30 January 2020 / Published online: 6 February 2020
© Springer Science+Business Media, LLC, part of Springer Nature 2020

Abstract

The discharge in mixtures of inert gas with sulfur vapors is an effective source of radiation spectrum, which is similar to solar in the wavelength range of 280–600 nm due to strong emission of S_2 molecules ($B^3\Sigma \rightarrow X^3\Sigma$ -transition). This phenomenon is utilized in microwave sulfur lamp. Despite a number of advantages microwave sulfur lamps have disadvantages that prevent their widespread use. This paper presents optical properties of the pulsed-periodic discharge in mixtures of argon with sulfur vapour in UV and visible spectral region and a global model of the discharge. Emission of the pulsed-periodic discharge in argon–sulfur vapour mixtures was studied at argon pressure up to 100 Torr and pressure of sulfur saturated vapors determined by temperature of gas-discharge tube walls varied due self-heating from the room temperature up to 160 °C. It is shown that strong band of S_2 molecules are observed in the discharge emission in the wavelength range of 300–600 nm and S and Ar lines are predominate in the wavelength range of 600–1000 nm. Effect of the discharge conditions on emission spectra was investigated. Time profiles of plasma species densities under various Ar– S_2 mixture compositions and voltage pulse up to 15 kV with duration $\sim 10 \mu s$ were calculated using the global model. It is shown, that densities of S_2^* molecules fast increases at the voltage pulse beginning and reach maximum after $\sim 2 \mu s$, so strong radiation of S_2^* is characteristic for the time interval, then S_2^* density fast decreases.

Keywords Longitudinal pulsed-periodic discharge · Argon–sulfur vapour mixtures · Optical properties · S_2 -emission · The global model · Species kinetics

✉ S. V. Avtaeva
s_avtaeva@mail.ru

A. A. Heneral
heneral@i.ua

¹ Institute of Laser Physics, SB RAS, Lavrentyeva Avenue 15B, Novosibirsk, Russia 630090

² Institute of Electronic Physics, National Academy of Sciences of Ukraine, Universitetskaya 21, Uzhgorod 88017, Ukraine

Introduction

Low-temperature plasmas of gas discharges have a wide range of practical applications including surface treatment [1, 2], plasma chemistry [3], plasma medicine [4], and light sources [5, 6]. Light is very important for life. The quality of life, health and urban safety associated with traffic and crime prevention depend on the light and its quality [7]. It worth noting, at the moment there is no light source that would fully satisfy all the requirements for light sources. Therefore, attempts to improve the existing types of sources, to develop fundamentally new or previously considered unpromising light sources continue. The important task is creation of radiation sources with high quality spectrum and high efficiency. The problem of creating high quality light sources not loses its relevance. All known light sources, such as incandescent, fluorescent, halogen, mercury, sodium, metal halide, xenon, sulfur and LED lamps have, along with advantages, significant disadvantages [7].

One of interesting directions to improve lighting systems is plasma lamps using radiation of sulfur vapour. Discharges in noble gas mixtures with sulfur vapor allow obtaining the radiation spectrum, caused by radiation of S_2 dimers, being similar to solar. S_2 dimer bands of the $B^3\Sigma \rightarrow X^3\Sigma$ system are approximately on equal distances from each other and merge in a continuous spectrum in the wavelength range of 280–600 nm. Using this technology, it is possible to create light sources with high luminous efficiency and high-quality spectrum that, in addition, do not require special recycling measures [7–12].

Sulfur lamps were developed by M. Ury and C. Wood in 1990 and the first really working sample of the sulfur lamp was demonstrated in 1992 [13, 14]. Serial production of plasma lamps was launched in 2010 [12]. The characteristics of such discharges have been studied since the 70 s both experimentally [15–19] and theoretically [20–23].

Important advantages of sulfur lamps are their environmental friendliness, high quality of the radiation spectrum and high energy-efficiency (light output up to ~ 100 lm/W). Sulfur lamps are much more environmentally friendly than mercury, metal-halogen or luminescent lamps, they do not contain neither mercury, nor lead, nor arsenic, as for example, the lamps studied in [24–26]. Sulfur vapor lamps are environmentally friendly, such as water vapor lamps [27, 28], but sulfur lamps have several advantages in comparison with the water vapor lamps. It is believed that sulfur lamps can be put on the same environmental step with LEDs. The emission spectrum of sulfur lamps in its spectral composition is very similar to the natural light emitted by the sun, with a sharply reduced level of radiation in the UV and IR ranges and with a maximum in the range of visible radiation, which is due to the properties of sulfur molecules that emit molecular bands mainly in the visible region of spectrum [8, 14].

However, despite a number of advantages, the microwave sulfur lamps have disadvantages that prevent their widespread application. The disadvantages of these lamps include the complexity of the design, the high cost of the lamp module, the high temperature of vapour in the bulb, hence the need to use a high-quality quartz glass and dust protection, using microwave radiation, an inertia, a large diameter of the luminous body (25–30 mm), which complicates focusing and using in optical systems [10].

The prerequisites for obtaining effective spontaneous luminescence of the gas-discharge plasma based on mixtures of sulfur vapors with argon are: (1) the presence of displaced $B^3\Sigma$ and $X^3\Sigma$ electronic states, which, according to the Frank–Condon principle, are essential for producing radiation between certain rovibronic states; (2) the dissociation limit of the main $X^3\Sigma$ term of the S_2 molecule is above the bottom of the potential well of

the excited $B^3\Sigma$ state [29], and therefore, the discharge energy should be directed mainly on excitation than on dissociation, which means that the discharge energy with high efficiency will be converted into spontaneous emission of the $B^3\Sigma \rightarrow X^3\Sigma$ transitions of S_2 molecules.

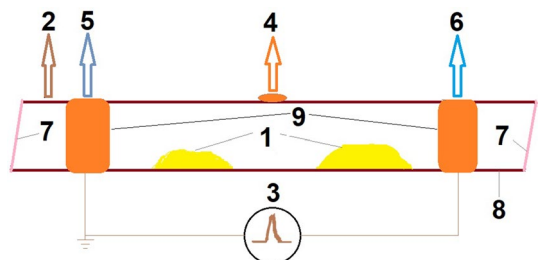
This paper presents properties of the pulse-periodic discharge in mixtures of argon with sulfur vapors studied experimentally and by modeling in the frame of a global model. “**Experiment**” section presents experimental setup and experimental findings. The discharge global model is described in “**Global model**” section. “**Results and discussion**” section includes basic results of modeling and discussion. In conclusions there are our findings and deductions.

Experiment

Luminescence of the sulfur vapour based plasma was excited by the longitudinal pulsed-periodic discharge in inert gas argon [29]. A sketch of the gas-discharge tube (GDT) is shown in Fig. 1. The experimental setup are described in detail elsewhere [25, 27]. The gas discharge tube was made from fused silica with inner diameter of 12 mm. Cuprum coaxial electrodes were disposed on opposite ends of the gas-discharge tube. A gap length between the coaxial electrodes was 25 cm. Sulfur powder of 99% purity was scattered over inner bottom side of the GDT. The radiation source was operated in a continuous pumping-out regime. The residual pressure was less than 10^{-1} Pa. The GDT was pumped out using the rotary vane vacuum pump. Pressure of sulfur saturated vapors in the GDT was determined by temperature of tube walls. The temperature control of the GDT walls was performed using the Pt-(Pt+Rh) thermocouple placed on the outer surface of the GDT wall near the center of the inter electrode distance. The temperature was varied due self-heating in a range from the room temperature up to 160 °C.

Dependence of the sulfur saturated vapor pressure on temperature was measured experimentally and is available in handbooks, for example [30]. The saturated vapour pressure of sulfur including all gaseous allotropes of sulfur increases from $\sim 10^{-6}$ Torr at temperature of 20 °C up to ~ 0.4 Torr at temperature of 160 °C. The GDT wall temperature was measured with the thermocouple on outer side of the wall. According to our estimations using the thermal conductivity equation temperature on the inner wall of the GD tube exceeds the temperature of the outer wall on $\sim 4^\circ\text{--}5^\circ$. In addition, temperature of the sulfur powder surface at boundary with gas phase according to the estimation can be higher than the inner wall temperature on $10^\circ\text{--}15^\circ$ due to low thermal conductivity of sulfur (0.27 W/(m K)). Therefore temperature of the sulfur powder surface is higher on about $15^\circ\text{--}20^\circ$ than the

Fig. 1 Sketch of the gas discharge tube (GDT): 1 is sulfur powder, 2—to pumping and argon inlet, 3 is GDT power source, 4—to thermocouple, 5—to voltage divider, 6—to current shunt, 7 are observation windows, 8 are quartz walls of the lamp, 9 are coaxial electrodes



temperature measured by the thermocouple. Taking into account the temperature correction the sulfur vapour pressure in the GD tube is varied from $\sim 10^{-5}$ Torr at wall temperature of 20 °C up to ~ 1 Torr at wall temperature of 160 °C. In captions to Figs. 3, 4, 5 and 6 the temperature measured by thermocouple is shown. The sulfur saturated vapor pressure was estimated by dependence of the sulfur saturated vapor pressure on temperature [30] using the temperature corrected on the estimated difference between temperature of outer side of the GDT wall and temperature of the sulfur powder surface.

For excitation of the longitudinal pulsed-periodic discharge in the emission source we used a generator with a resonant charge-exchange of the storage capacitor of 1650 pF and a thyatron serving as a switch. The oscillator ensured the pulse repetition frequency of 10 kHz at charging voltages of ≤ 10 kV.

The discharge radiation was observed through quartz windows, which passed up to 85% of the radiation at wavelength 200 nm. The spectral characteristics of the pulsed-periodic discharge were registered with the MS 7504i monochromator manufactured by Solar TII. The monochromator was equipped with three gratings (2400 lines/mm with a maximum spectral sensitivity at 270 nm; 1800 lines/mm with a maximum spectral sensitivity at 400 nm; 1200 lines/mm with a maximum spectral sensitivity at 600 nm) and the photo-multiplier tube PMT R928 (Solar TII). Spectral resolution of the MS 7504i was specified automatically and in our experiment was not higher than 0.1 nm. The recording system was calibrated using the photometric tungsten band lamp. Time integrated spectra of the discharge luminescence were recorded by the CCD camera HS 101H (Solar TII) conjugated with a computer.

Temporal emission characteristics of the pulse-periodic discharge plasma were recorded with the grating monochromator MDR-6 (LOMO, St. Petersburg) equipped by a photo-multiplier, a signal from which was output to one of oscilloscope channels. A coaxial low-resistance shunt with a resistance of 0.05 Ω and an RC voltage divider with a division factor of 400 served as sensors of current and voltage pulses, correspondingly. The maximum duration of current pulses was several μ s. Typical oscillograms of voltage pulses applied to the gas-discharge tube and current pulses through the discharge are shown in Fig. 2.

One of a typical luminescence spectra emitted by the pulse-periodic low-pressure discharge in mixture of argon with sulfur vapors is shown in Fig. 3. At the very beginning after switching on the discharge, when the tube wall temperature was \sim several tens of °C, argon atom lines were predominantly observed in the emission, and only when the discharge tube was self-heated up to 50 °C or more, the S_2 ($B^3\Sigma \rightarrow X^3\Sigma$) dimer bands appear, first in the ultraviolet and near to the infrared region of the spectrum, while the radiation intensity of argon atoms sharply reduces. The observed luminescence bands in the discharge spectrum are emitted due to fragmentation of sulfur polymers (S_3 – S_8), as a result of which excited S_2 ($B^3\Sigma$) molecules, as well as sulfur atoms, appear. The formation of excited sulfur species in a gas discharge is believed occurs under the influence of metastable argon atoms Ar_m with energy of ~ 11 eV; as it is well known, dissociation of sulfur molecules by electron impact begins at electron energies of ~ 10 eV [31]. Due to luminescence bands of the ($B^3\Sigma \rightarrow X^3\Sigma$) system of S_2 molecules are located approximately at the same distance from each other they merge into a continuous spectrum in the region of 280–600 nm, which maximum shifts to longer wavelengths, when the discharge tube is heated.

The maximum intensity of the spectral transition $3s^23p^3(^4S^\circ)4p \rightarrow 3s^23p^3(^4S^\circ)4s$ of the sulfur atom with a maximum at 921 nm was observed at the argon pressure ~ 14 Torr as it is shown in Fig. 4. It is worth noting that intensity of the $B^3\Sigma \rightarrow X^3\Sigma$ transition of S_2 sulfur molecules was maximum at argon pressures not exceeding 10 Torr. That

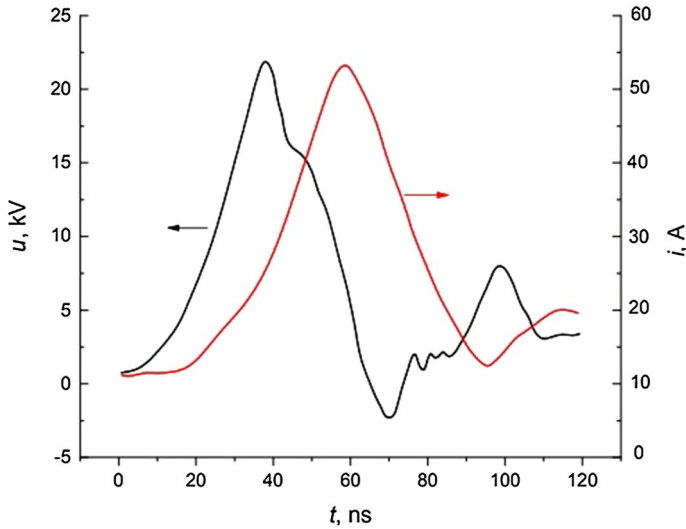
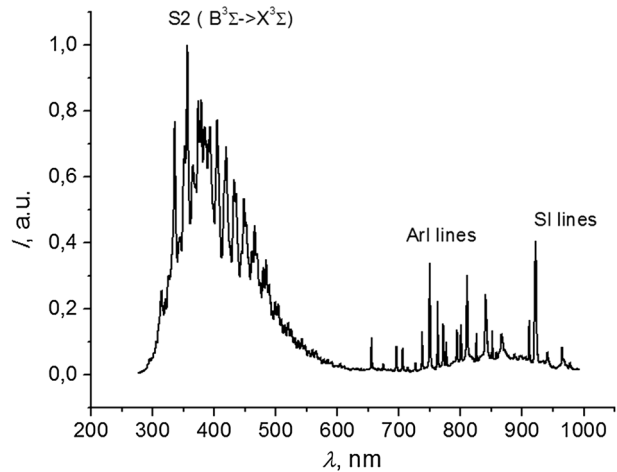


Fig. 2 Typical oscillograms of current and voltage pulses of the pulse-periodic low-pressure discharge in mixtures of argon with sulfur vapors

Fig. 3 The integrated over time emission spectrum of the high-voltage pulse-periodic discharge in mixture of Ar with sulfur vapors at power deposited in the discharge plasma ~ 200 W, argon pressure of 10 Torr, sulfur pressure is ~ 0.1 Torr and GDT wall temperature of 105°C



is, as the pressure of the argon–sulfur mixture decreases, an increase in the intensity of S_2 molecules and an increase in the number of electron–vibrational bands of the $B^3\Sigma^- \rightarrow X^3\Sigma^+$ transition of S_2 were observed, as well as a sharp decrease in the radiation intensity of excited argon atoms. This is a result of the interaction of S_2 molecules with metastable argon atoms and the manifestation of vibrational relaxation processes within the $B^3\Sigma^-$ and $X^3\Sigma^+$ states of S_2 molecules [29]. When the interaction happens, sulfur molecules are formed in two excited states $B^3\Sigma^-$ and $B'^3\Pi$, between which vibrational relaxation and exchange reactions are occurred, as a result, sulfur dimers emit in the radiative $B^3\Sigma^- \rightarrow X^3\Sigma^+$ transition.

Fig. 4 The radiation intensities of the $B^3\Sigma \rightarrow X^3\Sigma$ transition of sulfur molecules S_2 (1) and the $3s^23p^3(^4S^\circ)4p \rightarrow 3s^23p^3(^4S^\circ)4s$ transition of sulfur atoms (2) as functions of argon pressure; sulfur pressure is ~ 0.1 Torr and the GDT wall temperature is $95\text{--}105^\circ\text{C}$

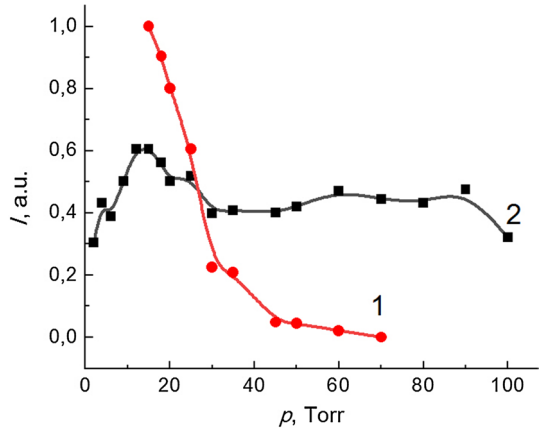


Fig. 5 The radiation intensities of the S_2 molecule band ($B^3\Sigma \rightarrow X^3\Sigma$ transition) (1) and the S atom line ($3s^23p^3(^4S^\circ)4p \rightarrow 3s^23p^3(^4S^\circ)4s$ transition) (2) as functions of the excitation frequency of the argon–sulfur mixture; argon pressure is 10 Torr, sulfur pressure is ~ 0.05 Torr, and the discharge tube temperature is $80\text{--}90^\circ\text{C}$

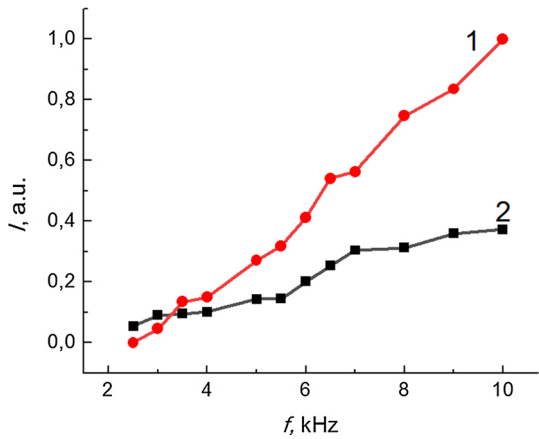


Fig. 6 The emission intensity of the S_2 molecule band ($B^3\Sigma \rightarrow X^3\Sigma$ transition) as a function of the GDT wall temperature at argon pressure of 10 Torr; sulfur vapour pressure increases with the wall temperature from $\sim 10^{-6}$ Torr at 20°C up to ~ 0.15 Torr at 120°C

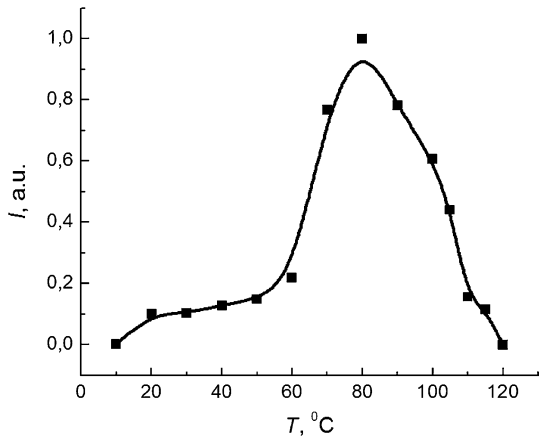


Figure 5 shows dependencies of the radiation intensities of the S₂ molecule band ($B^3\Sigma \rightarrow X^3\Sigma$ transition) and the S atom line ($3s^23p^3(^4S^\circ)4p \rightarrow 3s^23p^3(^4S^\circ)4s$ transition) on the excitation frequency of the argon–sulfur mixture. One can see, when the discharge frequency increases, the intensity of S₂ molecule radiation rises sharply due to increase in energy input to the plasma. Unfortunately, in our experiments it was not possible to raise the discharge excitation frequency more than 10 kHz.

The dependence of the emission intensity of the S₂ ($B^3\Sigma \rightarrow X^3\Sigma$) band on temperature of the discharge tube walls is shown in Fig. 6. The discharge plasma heats the gas-discharge tube walls to temperatures above 50 °C, and the intensity of the atomic sulfur spectral line with a maximum at 921 nm sharply increases. Simultaneously with an increase in the temperature to 80 °C, a visible radiation in the region of 300–600 nm increases, the discharge luminescence becomes whitish, and intensity of the sulfur atom resonance line $3s^23p^3(^4S^\circ)4p \rightarrow 3s^23p^3(^4S^\circ)4s$ falls several times, as does intensity of argon atom lines. As the temperature rises to 120 °C, the luminescence intensity of the S₂ ($B^3\Sigma \rightarrow X^3\Sigma$) band decreases sharply. At the discharge tube temperature of about 140–160 °C, the discharge was being extinguished altogether. A possible reason for this is the contraction of the discharge, which may be because of a lot of electronegative ions of sulfur polymers are effectively formed under these conditions, leading to discharge quenching.

Global Model

The global (0D) model was based on solution of the kinetic equations for plasma species and an equation of the electron energy balance [27, 32]. It is a difficult task to measure species densities in the Ar-sulfur vapour plasma; therefore calculation of the densities allows to receive the valuable information on plasma composition depending on the electric field and time.

The electron kinetics is described by balance equations for electron density

$$\frac{\partial n_e}{\partial t} = S_e - \frac{D_a}{A^2} \cdot n_e, \tag{1}$$

and energy

$$\frac{\partial n_e \epsilon}{\partial t} = -e\Gamma_e E - Q_{el} - Q_{inel}; \quad \Gamma_e = -\mu_e E n_e \tag{2}$$

here n_e , Γ_e , $\mu_e(\epsilon)$, ϵ are electron density, flux, mobility, and mean energy, respectively; $D_a(E/n)$ is ambipolar diffusion coefficient, S_e is the inter-particle collision source term for electrons; $Q_{el} = \sum_j \frac{2m}{M_j} \cdot k_{el,j} n_e n_j \epsilon$, $Q_{inel} = \sum_j \Delta \epsilon_j k_j n_e n_j$ are electron energy losses in elastic and inelastic collisions; m is mass of electrons, M_j is mass of atoms and molecules, $k_{el,j}$ is the rate constant of momentum transfer at elastic collisions of electrons with atom and molecules; $\Delta \epsilon_j$, k_j are the threshold energy and rate constant of a j th inelastic process respectively; A is the characteristic diffusion length defined by expression $\frac{1}{A^2} = \left(\frac{2.4}{R}\right)^2 + \left(\frac{\pi}{L}\right)^2$, R is the gas discharge tube radius, L is the distance between electrodes; E is electric field intensity; n is the total density of all neutral species; e is the elementary charge; t is time.

According to our estimations the electron energy loss in the discharge volume is much greater than its energy loss in the sheath region therefore the last was not taken into

account. Really, the maximal frequency of the diffusion loss in our discharge, estimated as $D_a/\Lambda^2 = T_e D_i/T_i \Lambda^2$, is $\approx (2-5) \times 10^6 \text{ s}^{-1}$ and the key volume loss of the electron energy in the discharge is S_2 excitation ($\Delta E = 5.03 \text{ eV}$) with frequency $k_{I0} n_{S2} \approx (2.14-8.56) \times 10^8 \text{ s}^{-1}$, that in about 100 times greater than the frequency of the diffusion loss.

The balance equations for positive and negative ion densities have a form

$$\frac{\partial n_{i,j}}{\partial t} = S_{i,j} - \frac{D_a}{\Lambda^2} \cdot n_{i,j}, \quad (3)$$

where $n_{i,j}$, $S_{i,j}$ are density and the inter-particle collision source term for j th sort ions, respectively.

The balance equations for neutral species are

$$\frac{\partial n_j}{\partial t} = S_j. \quad (4)$$

Here n_j and S_j are density and the inter-particle collision source term for j th sort neutral species.

The diffusion of electrons and ions is assumed with diffusion coefficient $D_a = \gamma \cdot D_i$, where $\gamma = \frac{T_e}{T_i}$, T_e is electron temperature $T_e = \frac{2}{3k_B} \bar{\epsilon}$ (k_B is the Boltzmann constant), $T_i = T_{\text{gas}}$ is ion temperature and $D_i = \frac{1}{m} \sum_j D_{ij}$; here D_{ij} is diffusion coefficient of the j th sort of ions and m is number of ions sorts. The same diffusion coefficient D_a was utilized for all charged particles to conserve plasma quasi-neutrality. It is reasonable approximation as the volume loss of electrons dominates in the discharge, which means that the sheath volume is small. Diffusion coefficients of each sort of ions were estimated by the expression $D_{ij} = \frac{\pi v_j \lambda_j}{8}$, where v_j is the thermal velocity of the particles, $\lambda_j = ((1 - \chi)n_{Ar} \pi (a_j + a_{Ar})^2 + \chi n_{S2} \pi (a_j + a_{S2})^2)^{-1}$ is the mean free path, and χ is S_2 fraction in Ar- S_2 mixture. Here n_{Ar} and n_{S2} are densities of Ar atoms and S_2 molecules, a_j , a_{Ar} and a_{S2} are radii of the j th sort of ions, Ar atoms and S_2 molecules.

Diffusion of neutral species was not taken into account in the model because of the following reasons. Diffusion of excited species S_2^* , S^* , Ar_r^* and Ar^{**} did not considered since their life times are small and they are mostly lost due to radiative decay in the discharge column. Diffusion of the metastable argon atoms Ar_m was not taken into account because of high rates of Ar_m conversion into Ar_r^* and Penning ionization (reactions 5 and 7 in Table 2) compared with the diffusion rate. Diffusion of S atoms was ignored due to lack of information about their recombination on the GDT walls.

Species considered into the kinetic scheme are presented in the Table 1. The kinetic scheme is presented in the Table 2.

Sulfur polymers (S_3-S_8) are not considered in the kinetic scheme due to following reasons: (1) there is very lack in cross sections (rate constants) for electron collisions with sulfur polymers and for mutual collisions of various sulfur polymer species; (2) during the passage of a current pulse through the gas-discharge tube, the gas is instantaneously heated

Table 1 Species of Ar- S_2 plasma considered in the kinetic scheme

Neutral species	Ar	S_2	S		
Excited species	Ar_m	Ar_r^*	Ar^{**}	S_2^*	S^*
Positive ions	Ar^+	S_2^+	S^+		
Negative species	S_2^-	S^-	e^-		

Here S_2^* is sulfur dimer in the excited state $S_2 (B^3 \Sigma_u^-)$

Table 2 Reactions of Ar–S₂ plasma considered in the kinetic scheme

No.	Reaction	Rate constant, m ³ⁿ /s (n = 0, 1, 2)	References
1	e + Ar → e + Ar	k ₁ (ε)s	[35]
2	e + S ₂ → e + S ₂	k ₂ (ε)	[36]
3	e + Ar → Ar _m + e	1.0 × 10 ⁻¹⁷ · T _e ^{0.75}	[37]
4	e + Ar → e + Ar**	5.0 × 10 ⁻¹⁸ · T _e ^{0.5}	[37]
5	e + Ar _m → e + Ar _r *	2.0 × 10 ⁻¹³	[38]
6	e + Ar → 2e + Ar ⁺	K ₆ (ε)	[35]
7	Ar _m + Ar _m → e + Ar ⁺ + Ar	1.2 × 10 ⁻¹⁵	[39]
8	2e + Ar ⁺ → e + Ar	5.4 × 10 ⁻³⁹ / T _e ^{4.5}	[40]
9	e + Ar ⁺ + Ar → Ar + Ar	2.3 × 10 ⁻³⁴ / T _e ^{2.5}	[41]
10	e + S ₂ → e + S ₂ *	k ₁₀ (ε)	[42]
11	e + S ₂ → 2e + S ₂ ⁺	k ₁₁ (ε)	[43]
12	e + S ₂ → S ₂ ⁻	k ₁₂ (ε)	[44]
13	e + S ₂ → S ⁻ + S	k ₁₃ (ε)	[44]
14	2e + S ₂ ⁺ → e + S ₂	3.3 × 10 ⁻³⁰ · k ₁₁ (ε) · exp(9.31/T _e) · (T _e /Ry) ^{-1.5}	[45]
15	e + S ₂ ⁺ → S + S	3.0 × 10 ⁻¹⁴ / T _e ^{0.5}	[45]
16	e + S → e + S*	k ₁₆ (ε)	[46]
17	S ₂ ⁻ + S ₂ ⁺ → S ₂ * + S ₂	2.92 × 10 ⁻¹⁴	[45]
18	S ⁻ + S ₂ ⁺ → S ₂ * + S	3.21 × 10 ⁻¹⁴	[45, 47]
19	S ₂ ⁻ + Ar ⁺ → S ₂ + Ar**	3.33 × 10 ⁻¹⁴	[45, 47]
20	S ⁻ + Ar ⁺ → S + Ar**	3.51 × 10 ⁻¹⁴	[45, 47]
21	S ⁻ + S ⁺ → S + S*	3.7 × 10 ⁻¹⁴	[45, 47]
22	Ar ⁺ + S → Ar + S ⁺	4.72 × 10 ⁻¹⁶	[45]
23	S + S + Ar → S ₂ + Ar	3.22 × 10 ⁻⁴³	[45]
24	Ar** + Ar → Ar _m + Ar	1.0 × 10 ⁻¹⁶	[37]
25	Ar** + Ar → Ar _r * + Ar	1.0 × 10 ⁻¹⁶	[37]
26	Ar _r * → Ar	2.0 × 10 ⁶	[48]
27	Ar** → Ar	3.0 × 10 ⁷	[48]
28	S ₂ * → S ₂	5.3 × 10 ⁷	[49]
29	S* → S	1/τ	[50]

$$T_e = \bar{\epsilon} / 1.5$$

to high temperatures on the order of several hundred Celsius degrees and fractions of sulfur polymer are significantly reduced. All calculations were carried out for a gas temperature of ~800 °C, at which the fraction of S₂ molecules in sulfur vapor becomes the main one [33, 34].

The rate constants of reactions 1, 2, 6, 10–13 and 16 in the Table 2 were calculated by averaging cross sections of corresponding reactions on the electron energy distribution function (EEDF).

The EEDF was calculated using program BOLSIG + [51], cross sections of electron collisions with sulfur molecules and atoms were taken from [36, 42–44, 46, 52], cross sections of electron collisions with argon atoms were taken from [35, 53]. A rate constant of three-body recombination of S₂⁺ ions (reaction 14 in Table 2) was calculated by principle of detailed equilibrium as

$$k_r = k_i \frac{g_0}{g_i} \frac{4\pi^{3/2} a_0^3}{(T_e/Ry)^{3/2}} e^{\frac{E_i}{T_e}}, \quad \text{where } Ry = 13.606 \text{ eV} \quad (5)$$

The rate constant k_i in (5) corresponds to rate constant of the reaction 11 in Table 2 as it is shown in the Table.

Rate constants of mutual neutralization of positive and negative ions were estimated by the Coulomb interaction model [45, 47] and rate constant of charge transfer from Ar^+ ions to S atoms was estimated as $k = \pi e(\alpha/\mu)^{1/2}$, where α is atom polarizability, μ is reduces mass of colliding species and e is electron charge [45].

The model equations represent a stiff system of the ordinary differential equations. The system was solved using the VODE software package [54].

The simulations were performed for experimental conditions similar to studied in [29]. Initial densities of Ar atoms and S_2 molecules were calculated as $n = P/kT$; initial densities of other neutral species were set to zero. Initial densities of electrons and Ar^+ ions were set as $10^9\text{--}10^{11} \text{ m}^{-3}$; initial densities of other ions were set to zero.

Results and Discussion

Figure 7a shows the mean electron energies in discharges in Ar– S_2 mixtures as functions of reduced electric field at fraction of S_2 vapors in the mixture of 0.5–10%. Figure 1b shows a critical (breaking) electric field E^*/n , at which total ionization rate equals total attachment rate, as a function of S_2 vapour fraction in the mixtures. One can see, that increasing the S_2 molecule fraction in Ar– S_2 mixtures promotes decrease in the mean electron energy and increase in the breaking field, at which a transition from electronegative to electropositive plasma takes place.

Ionization and attachment rate constants as functions of the reduced electric field E/n at S_2 fraction in Ar– S_2 mixtures 2 and 5% are shown in Fig. 8. One can see, increase in the E/n and in the mean electron energy leads to rising the ionization and excitation rate constants of both S_2 molecules and Ar atoms as well as to diminution of rate constants of the electron attachment to sulfur molecules and atoms. Increasing sulfur fraction in Ar– S_2 mixtures results in rising rate constants of electron attachment to sulfur molecules and atoms and diminishing the ionization and excitation rate constants of these species.

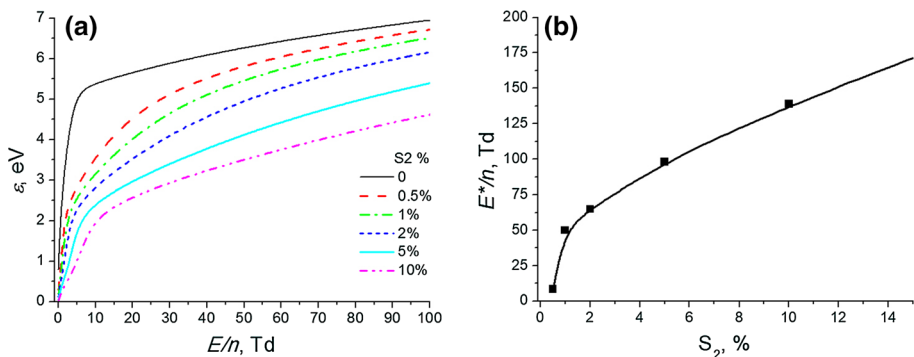


Fig. 7 a Dependencies of the mean electron energy on the reduced electric field at varied sulfur fractions in Ar– S_2 mixtures, b the critical electric field as a function of S_2 fraction in the mixtures

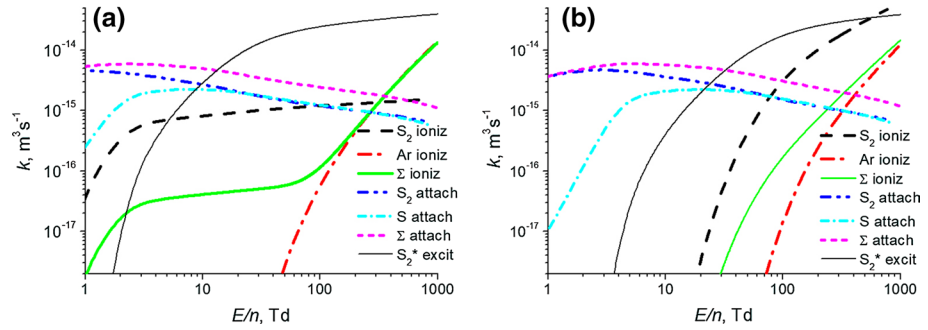


Fig. 8 Ionization and attachment rate constants as functions of the reduced electric field in **a** 99%Ar–1% S_2 and **b** 95%Ar–5% S_2 mixtures; $k_{i\Sigma} = \sum (\chi k_{iS_2} + (1 - \chi)k_{iAr})$, where k_{iS_2} and k_{iAr} are ionization rate constants of S_2 and Ar (reactions 11 and 6), correspondingly, and χ is S_2 fraction in Ar– S_2 mixture; $k_{a\Sigma} = \sum (k_{aS_2} + k_{aS})$, where k_{aS_2} and k_{aS} are electron attachment rate constants to S_2 and S (reactions 12 and 13)

Figure 9 shows shape of voltage pulse used for calculations of the discharge in 99%Ar–1% S_2 mixture as well as the E/n and the mean electron energy evolution during the voltage pulse; the voltage pulse was utilized in form $2U_0/(exp(t/\tau_p) + exp(-t/\tau_p))$.

Figure 10 shows evolution of charged and neutral species densities in 99%Ar–1% S_2 mixture during voltage pulse in nearly steady state regime. One can see, during the pulse beginning the plasma is strong electronegative: electron density is much less than density of ions (more than 500 times), primary positive ions are Ar^+ ions and primary negative ions are S_2^- ions, densities of S_2^+ , S^- and S^+ ions are much less than densities of Ar^+ and S_2^- ions (Fig. 10b). But, during first two μ seconds electrons density fast increases reaching values of $\sim 2 \cdot 10^{19} m^{-3}$ after about 2–3 μ s; at this their energy decreases a little (3–4%) while E/n decreases on $\sim 10\%$. The increase in electron density leads to an increase in all other species: both ions and neutrals. Densities of S_2^+ and S^- ions grow quicker than S_2^- and Ar^+ ion densities, so after $\sim 1 \mu$ s S_2^+ ions become the primary positive ions and densities of negative S_2^- and S^- ions are about equal. Then densities of all species excluding S atoms decrease due decreasing E/n and the mean electron energy (Fig. 9b). Density of S_2^+

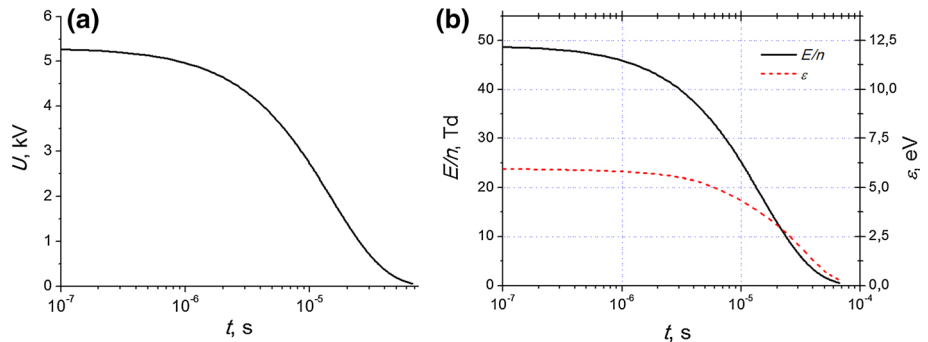


Fig. 9 a Voltage pulse shape and **b** dependencies of the reduced electric field (E/n) and the mean electron energy (ϵ) on time during the voltage pulse; $U_0 = 5.6$ kV, $\tau_p \sim 10 \mu$ s, $P_{Ar} = 40$ Torr, $P_{S_2} = 0.4$ Torr ($\sim 1\%$ S_2 in Ar– S_2 vapour mixture)

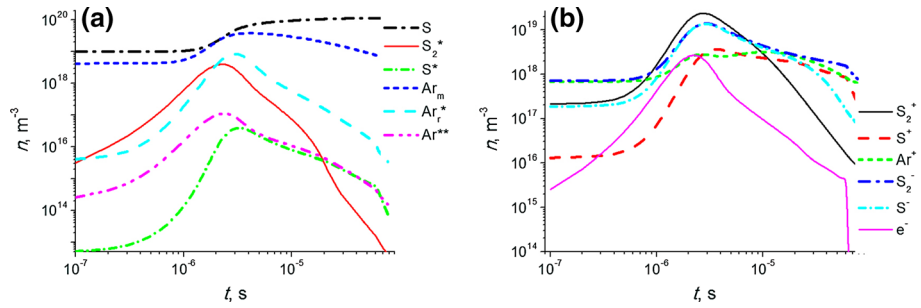


Fig. 10 Dependencies of neutral (a) and charged (b) species densities on time during the voltage pulse; $U_0=5.6$ kV, $\tau_p \sim 10 \mu\text{s}$, $P_{\text{Ar}}=40$ Torr, 1% S_2 in Ar– S_2 vapour mixture

ions decreases faster than densities of other ions. After about 7–9 μs Ar^+ ions are primary positive ions again and S^- density is less than S_2^- density anew.

Short-lived excited species (Ar_r^* , Ar^{**} , S_2^* , S^*) densities behave like the electron density: reach their maximum values after about 2–3 μs from voltage pulse beginning and then decrease (Fig. 10a). Densities of S atoms and metastable Ar atoms start grow only after 1 μs , when the electron density reached a great enough value, and then decrease a little; their densities are much higher than densities of short-lived species. During most part of the period densities of S_2^* and Ar_r^* are much higher than densities of Ar^{**} and S^* atoms; only after about 20 μs from voltage pulse beginning S_2^* density falls down to S^* density. At high enough mean electron energy S_2^* density exceeds Ar_r^* density while with diminishing electron energy S_2^* density fast decreases and Ar_r^* density becomes higher S_2^* density. So during first 10 μs the discharge emits S_2 bands as well as S and Ar (2p–1s) lines in visible part of spectrum; during the rest of the period S_2^* radiation fast decreases and discharge emits mostly S and Ar (2p–1s) lines while their intensities also decreases.

Figure 11 shows shape of voltage pulse used for calculations of the discharge in 95%Ar–5% S_2 mixture as well as evolution of the reduced electric field (E/n) and the mean electron energy during the voltage pulse; Fig. 12 shows evolution of charged and neutral

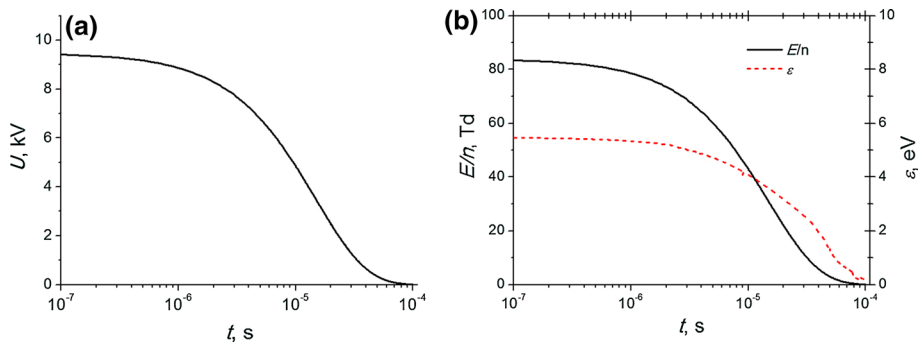


Fig. 11 Voltage pulse shape (a) and dependencies of reduced electric field (E/n) and mean electron energy (ϵ) on time during the voltage pulse (b); $U_0=10$ kV, $\tau_p \sim 10 \mu\text{s}$, $P_{\text{Ar}}=40$ Torr, $P_{\text{S}_2}=2.1$ Torr (5% S_2 in Ar– S_2 vapour mixture)

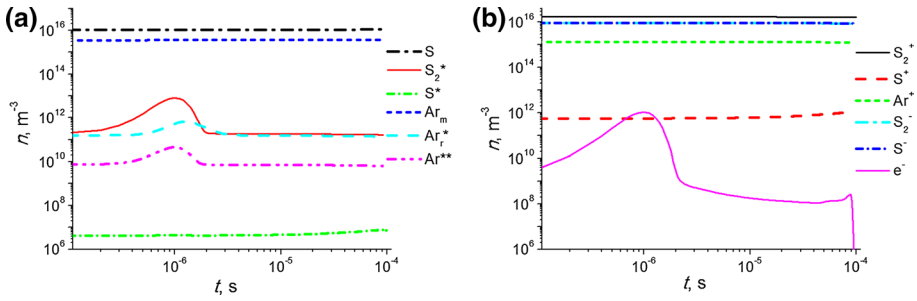


Fig. 12 Dependencies of neutral (a) and charged (b) species densities on time during the voltage pulse; $U_0=10$ kV, $\tau_p \sim 10$ μ s, $P_{Ar}=40$ Torr, $P_{S_2}=2.1$ Torr (5% S_2 in Ar– S_2 vapour mixture)

species densities in steady state. Figures 13 and 14 show the same dependencies for the discharge in 91%Ar–9% S_2 mixture.

Discharge properties and species kinetics in discharge at 5 and 9% S_2 in Ar– S_2 mixtures are different from the properties and kinetics in discharge at 1% S_2 . At the same time species kinetics in discharges at 5 and 9% S_2 in Ar– S_2 mixtures are similar while in mixture with 9% S_2 electronegative effects are more expressive compared with mixture with 5% S_2 .

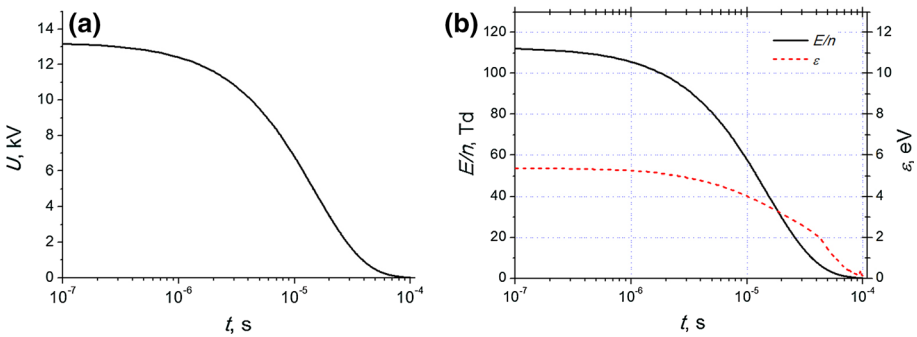


Fig. 13 a Voltage pulse shape and b dependencies of reduced electric field (E/n) and mean electron energy (ϵ) on time during the voltage pulse; $U_0=14.5$ kV, $\tau_p \sim 10$ μ s, $P_{Ar}=40$ Torr, $P_{S_2}=4$ Torr (9% S_2 in Ar– S_2 vapour mixture)

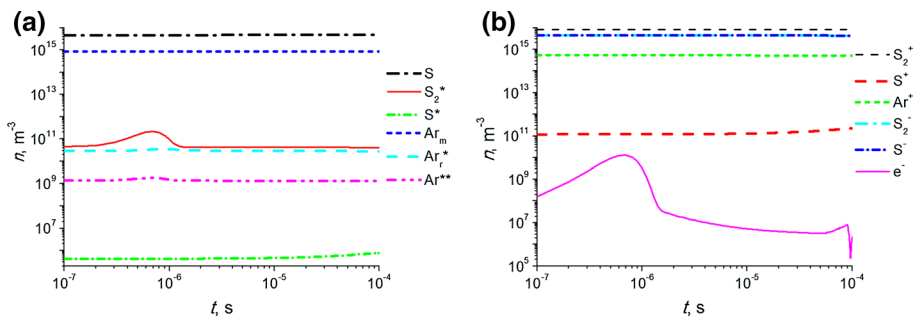


Fig. 14 Dependencies of neutral (a) and charged (b) species densities on time during the voltage pulse; $U_0=14.5$ kV, $\tau_p \sim 10$ μ s, $P_{Ar}=40$ Torr, $P_{S_2}=4$ Torr (9% S_2 in Ar– S_2 vapour mixture)

Electron density in discharges in these mixtures is much less than ion densities, the discharge plasma is very electronegative. After a short time after gas gap breakdown both positive and negative ion densities saturates and remains about unchanged during voltage pulse in steady state. The primary positive ions in electronegative Ar–S₂ plasma are S₂⁺ ions, densities of Ar⁺ and S⁺ ions are much less. The negative ions S₂⁻ and S⁻ are in commensurable amounts. Densities of S and Ar_m atoms also remain about unchanged during voltage pulse. Electron density and densities of short-lived excited species (Ar_r^{*}, Ar^{**}, S₂^{*}) in the pulse beginning increase and reach their maximum at about 1 μs then decrease.

Densities of all species despite more pulse voltage and reduced electric field needed for discharge ignition and maintenance are less at greater S₂ fraction in Ar–S₂ mixtures. At small S₂ fraction (≤ 1–2%) in Ar–S₂ mixtures ionization degree varies during voltage pulse reaching its maximum after about microsecond from pulse beginning. At great S₂ fraction (≥ 5%) in Ar–S₂ mixtures ionization degree remains about constant during whole pulse. Ionization degree of the plasma decreases with increase in S₂ fraction in Ar–S₂ mixtures. Electron density and densities of short-lived excited species (Ar_r^{*}, Ar^{**}, S₂^{*}) increase during first microsecond, reach maximum and then decrease. Emissivity of the discharge decreases with increasing S₂ fraction at this emission Ar lines decreases strongly as compared with emission of S₂ bands.

These findings are in accordance with experimental study of the pulse-periodic discharge in sulfur vapour/argon mixtures, which shows that with an increase in the GDT wall temperature above 80 °C, the discharge luminescence decreases, intensity of S and Ar lines falls several times; as the temperature rises to 120 °C, the S₂ band intensity decreases sharply and at the temperature of about 140–160 °C, the discharge is extinguished altogether. It is worth reminding that pressure of sulfur saturated vapors in the GDT was determined by temperature of tube walls, which was varied due self-heating. Herewith sulfur vapour pressure in the GDT was varied from ~ 10⁻⁵ Torr at 20 °C up to ~ 1 Torr at 160 °C. Therefore, at argon pressure of 10 Torr and wall temperature of ≤ 120 °C the sulfur vapour fraction in sulfur vapour/argon mixtures was ≤ 1%. At increase of wall temperature up to 160 °C the sulfur vapour fraction in the mixtures reached 10%.

The presence in the discharge negative ion species greatly complicates the analysis of particle and energy balance [55]. The diffusive loss is, in general, no longer ambipolar, but under certain conditions, the diffusive loss is ambipolar. As it was shown by Libermann [55] in this case ambipolar diffusion coefficient is function of $\gamma = T_e/T_i$ and $\alpha = n/n_e$, where T_i is temperature of ions and n_e is density of negative ions:

$$D_a \approx D_+ \frac{1 + \gamma + 2\gamma\alpha}{1 + \gamma\alpha}.$$

When $\alpha \gg 1$, γ cancels out such that $D_a \approx 2D_+$. When α decreases below 1, but $\gamma\alpha \gg 1$, $D_a \approx D_+/\alpha$. For $\gamma\alpha < 1$, $D_a \approx \gamma D_+$, which is the usual ambipolar diffusion coefficient without negative ions.

In our model we use $D_a \approx \gamma D_+$, which holds in case of $\gamma\alpha < 1$. In case of 0.99Ar–0.01S₂ mixture according to Fig. 10 $\alpha \approx 10$ –300 (in case of 5 and 9% S₂ α is higher) and $\gamma\alpha \gg 1$, what means that it will be more correct to use $D_a \approx 2D_+$. Therefore, the diffusion loss in the discharge is about one order of magnitude lower. However, this finding does not invalidate the simulation result because according with estimations the volume loss of charged species prevails in the discharge. In addition, simulations performed with different values of the ambipolar diffusion coefficient showed that changing the diffusion coefficient has little influence on the simulation results, which confirms the prevalence of the volume losses.

It worth noting, that for plasma in which $\alpha \gg 1$ in the centre of the discharge, the entire transition region takes place over a small range of $1/\gamma < \alpha < 1$ near the discharge surface, such that the simpler value of $D_a = 2D_+$ holds over most of the plasma, except very near the surface where negative ions density is zero [55].

The simulation results allow us to estimate frequencies of reactions (5) and (7) and compare them with frequency of diffusion loss Ar_m on the wall D_{Ar}/A^2 , which at our conditions equals 256 s^{-1} . Taking for discharge in 0.99Ar–0.01S₂ mixture $n_e = 2 \times 10^{15} - 3 \times 10^{18} \text{ m}^{-3}$, $n_{Ar_m} = 3 \times (10^{18} - 10^{19}) \text{ m}^{-3}$ (see Fig. 10), $k_5 = 2 \times 10^{-13} \text{ m}^3/\text{s}$ and $k_7 = 1.2 \times 10^{-15} \text{ m}^3/\text{s}$ we get the reaction (5) frequency $4 \times 10^2 - 6 \times 10^5 \text{ s}^{-1}$ and the reaction (7) frequency $3.6 \times (10^3 - 10^4) \text{ s}^{-1}$. Therefore in this case, rates of Ar_m conversion into Ar_r^* and Penning ionization are much higher compared with the diffusion rate and the simplification of the model with neglecting the Ar_m diffusion is valid. But already in 0.95Ar–0.05S₂ mixture with $n_e = 10^8 - 5 \times 10^9 \text{ m}^{-3}$, $n_{Ar_m} = 10^{11} - 10^{13} \text{ m}^{-3}$ (Fig. 11) we have the reaction (5) frequency $2 \times 10^{-5} - 10^{-3} \text{ s}^{-1}$ and the reaction (7) frequency $1.2 \times (10^{-4} - 10^{-2}) \text{ s}^{-1}$ that much less than the diffusion rate. So in case of 5 and 9% S₂ in Ar–S₂ mixtures, the simplification is not suitable and consequently densities of Ar excited species given by the model are overstated.

Conclusions

The discharges in argon–sulfur vapor mixtures are effective sources of radiation spectrum, close to solar in the wavelength range of 280–600 nm. The study of optical properties of pulsed-periodic discharge in argon–sulfur vapour mixtures shows that the discharge spectra contain emission of S₂ band in wavelength range of 300–600 nm as well as ArI and SI lines in wavelength range of 600–1000 nm. Also in UV region there are S⁺ lines which overlapped with S₂ bands. Increase in sulfur vapour fraction in these mixtures, which rises with the GDT wall temperature, results first in reaching an optimal S₂ emission and then in diminution of the discharge luminescence and finally in quenching of the discharge. Emission of S₂ bands is dominating emission at low argon pressure less than ~30 Torr and strongly dependent on sulfur vapour fraction in the mixtures (GDT wall temperature). Calculation of the Ar–S₂ plasma species kinetics show that during voltage pulse density of S₂^{*} (*B*³ Σ) molecules fast rises and exceeds densities of other excited species; however, when pulse voltage decreases and as a consequence energy of electrons diminishes, density of excited sulfur molecules prompt falls while density of resonance excited argon and sulfur atoms decreases slower. This is one of reasons for appearance of ArI and SI lines together with S₂ bands in spectra of the longitudinal pulsed-periodic discharge in sulfur vapor–argon mixtures. The simulation findings are in accordance with results of experimental study of Ar–S₂ pulsed periodic discharge spectra; the spectra mainly contain S₂ molecule bands as well as Ar and S lines in the visible part of spectrum.

The processes or the predominance of processes leading to the luminescence of sulfur dimers on the *B*³ $\Sigma \rightarrow X$ ³ Σ transition in the pulsed discharge, study of which was also presented in [29], remain incomprehensible. It is not clear, for example, does an “instantaneous” dissociative excitation or a “stepwise” excitation–dissociation of sulfur polymers dominate in the discharge. Therefore additional investigations, including more detailed modeling and study of Ar–sulfur plasma in different types of discharges, for example, in a dielectric barrier discharge are required.

Acknowledgements The authors are very grateful to Profs. V. A. Kelman and Yu. V. Zhmenyak for help in performing the experiments, advices and useful scientific discussions.

References

- Ricard A, Sarrette JP (2019) Densities of active species in R/x%(N₂–5%H₂) (R = Ar or He) microwave flowing afterglows. *PCPP* 39:1103–1114
- Yanez-Pacios AJ, Martín-Martínez JM (2018) Improved surface and adhesion properties of wood-polyethylene composite by treatment with argon-oxygen low pressure plasma. *PCPP* 38:871–886
- Malik MA, Hughes D, Malik A, Xiao S, Schoenbach KH (2013) Study of the production of hydrogen and light hydrocarbons by spark discharges in diesel, kerosene, gasoline, and methane. *PCPP* 33:271–279
- Su X, Feng M, Rogers S, Holsen TM, Mededovic Thagard S (2019) The role of high voltage electrode material in the inactivation of *E. coli* by direct-in-liquid electrical discharge plasma. *PCPP* 39:577–596
- Barjasteh A, Eslami E (2018) Numerical investigation of effect of driving voltage pulse on low pressure 90%Ar–10%Cl₂ dielectric barrier discharge. *PCPP* 38:261–279
- Baeva M, Reiter D (2003) Monte Carlo simulation of radiation trapping in Hg–Ar fluorescent discharge lamps. *PCPP* 23:371–387
- Zissis G, Kitsinelis S (2009) State of art on the science and technology of electrical light sources: from the past to the future. Topical review. *J Phys D Appl Phys* 42:173001
- Malkov M (2011) Sulfur lamp. A promising start and... an unpredictable future? Part I. A bit of history and about the lamp device. *Sovremennaya Svetotekhnika (Modern Lighting)* 3:69–72
- Malkov M (2011) Sulfur lamp. A promising start and... an unpredictable future? Part II. A little about the physics of sulfur discharge. *Sovremennaya Svetotekhnika (Modern Lighting)* 4:53–58
- Malkov M (2011) Sulfur lamp. A promising start and... an unpredictable future? Part III. Technical characteristics of lamps and light distribution systems. *Sovremennaya Svetotekhnika (Modern Lighting)* 5:69–72
- Müller P, Klán P, Církva V (2005) The electrodeless discharge lamp: a prospective tool for photochemistry Part 5: fill material-dependent emission characteristics. *J Photochem Photobiol, A* 171:51–57
- https://en.wikipedia.org/wiki/Sulfur_lamp
- Dolan JT, Ury MG, Wood CH (1992) Novel high efficacy microwave powered light source. VIth Intern Sym on the Science and Technology of Light Sources. Tech University Budapest (Lighting Sciences 6), pp 301–302
- Long-life “super lamp” mimics bright sunlight (1994) *Elec Rev* 22:18
- Childs AH, Schrenk WG (1976) Some characteristics of low pressure, sulfur, microwave-excited, electrodeless discharge lamps. *Appl Spectrosc* 30:507–509
- Turner BP, Ury MG, Leng Y, Love WG (1997) Sulfur lamps - progress in their development. *J Illum Eng Soc* 26:10–16
- Krizek DT, Mirecki RM, Britz SJ, Harris WG, Thimijan RW (1998) Spectral properties of microwave-powered sulfur lamps in comparison to sunlight and high pressure sodium/metal halide lamps. *Biotronics* 27:69–80
- Chen Y, Chen D (2006) Study the buffer gas for microwave sulfur lamp. In: Conf record of the 2006 IEEE industry applications conf forty-first IAS annual meeting. Tampa, FL, USA. <https://doi.org/10.1109/ias.2006.256746>
- Aleksandrova OYu, Bondarenko SM, Guttsayt EM, Zhidkov RA (2013) Plasma lighting devices based on microwave discharge. *T-Comm Telecommun Transp* 9:9–11
- Johnston CW (2003) Transport and equilibrium in molecular plasmas: the sulfur lamp. PhD Thesis: Technische Universität Eindhoven
- Van der Heijden HWP (2003) Modelling of radiative transfer in light sources. PhD Thesis: Technische Universität Eindhoven
- Van der Heijden H, Van der Mullen J, Baier J, Körber A (2002) Radiative transfer of a molecular S₂ B-X spectrum using semiclassical and quantum-mechanical radiation coefficients. *J Phys B: At Mol Opt Phys* 35:3633–3654
- Johnston CW, Van der Heijden HWP, Janssen GM, Van Dijk J, Van der Mullen JJAM (2002) A self-consistent LTE model of a microwave-driven, high-pressure sulfur lamp. *J Phys D Appl Phys* 35:342–351
- Heneral AA, Avtaeva SV (2017) Emission characteristics of plasma based on xenon-rubidium bromide mixture. *Opt Spectrosc* 123:531–534
- Heneral AA, Avtaeva SV (2017) Emission characteristics of Xe–RbBr plasma. *J Phys D Appl Phys* 50:495202

26. Heneral AA, Zhmenyak YV (2018) Luminescent characteristics of a pulsed discharge plasma in Xe–KBr mixture. *J Appl Spectrosc* 85:79–83
27. Avtaeva SV, General AA, Kel'man VA (2010) Kinetic model for low-density non-stationary gas discharge in water vapour. *J Phys D Appl Phys* 43:315201
28. Shuaibov AK, Heneral AA, Shpenik YuO, Zhmenyak YuV, Shevera IV, Gritsak RV (2009) Ultraviolet radiation sources on (H₂O, D₂O) water vapor. *Tech Phys* 54:1238–1240
29. General AA, Kelman VA, Zhmenyak YuV, Zvenigorodsky VV (2016) Optical radiation of a gas discharge in argon–sulfur mixture. *J Appl Spectrosc* 83:598–602
30. Kikoin IK (ed) (1976) Tables of physical quantities. Handbook (p 201). Atomizdat, Moscow
31. Zavilopulo AN, Shpenik OB, Markush PP, Mykyta MI (2014) *Tech Phys Lett* 40:13–17
32. Avtaeva SV, Avdeev SM, Sosnin EA (2010) Radiation of nitrogen molecules in a dielectric barrier discharge with small additives of chlorine and bromine. *Plasma Phys Rep* 36:719–728
33. Rau H, Kuttly TRN, Guedes de Carvalho JRF (1973) Thermodynamics of sulphur vapour. *J Chem Thermodyn* 5:833–844
34. Ferreira AGM, Lobo LQ (2011) The low-pressure phase diagram of sulfur. *J Chem Thermodyn* 43:95–104
35. PHELPS database <http://www.lxcat.laplace.univ-tlse.fr>
36. Tashiro M (2008) Exchange effects in elastic collisions of spin-polarized electrons with open-shell molecules with $^3\Sigma_g^-$ symmetry. *Phys Rev A* 77:012723
37. Johnson TH, Cartland HE, Genoni TC et al (1989) A comprehensive kinetic model of the electron-beam-excited xenon chloride laser. *J Appl Phys* 66:5707–5725
38. Bassett NL, Economou DJ (1994) Effect of Cl₂ additions to an argon glow discharge. *J Appl Phys* 75:1931–1939
39. Klucharev N, Vujnovic V (1990) Chemi-ionization in thermal-energy binary collisions of optically excited atoms. *Phys Rep* 185:55–81
40. Moravej M, Yang X, Barankin M, Penelon J, Babayan SE, Hicks (2006) RF properties of an atmospheric pressure radio-frequency argon and nitrogen plasma. *Plasma Sources Sci Technol* 1(5):204–210
41. Dyatko NA, Ionikh YZ, Kochetov IV, Marinov DL, Meshchanov AV, Napartovich AP, Petrov FB, Starostin SA (2008) Experimental and theoretical study of the transition between diffuse and contracted forms of the glow discharge in argon. *J Phys D Appl Phys* 41:055204
42. Tashiro M (2008) Electron impact excitations of S₂ molecules. *Chem Phys Lett* 453:145–149
43. Freund RS, Wetzel RC, Shul RJ (1990) Measurements of electron-impact- ionization cross sections of N₂, CO, CO₂, CS, S₂, CS₂, and metastable N₂. *Phys Rev A* 41:5861–5868
44. Coat YL, Bouby L, Guillotin JP, Ziesel JP (1996) Negative ion formation by electron attachment in S₂ and in the sulphur vapour. *J Phys B: At Mol Opt Phys* 29:545–553
45. Chernii GG, Losev SA (eds) (1995) Physico-chemical processes in gas dynamics. Vol 1 Dynamics of physico-chemical processes in gas and plasma. Moscow University Publishing, Moscow
46. Zatsarinny O, Tayal SS (2002) Electron impact collision strengths and rates for neutral sulphur using the *B*-spline *R*-matrix approach. *J Phys B: At Mol Opt Phys* 35:2493–2503
47. Elestskiy AV, Smirnov BM (2000) Elementary processes in plasma. In: Fortov VE (ed) Encyclopedia of low-temperature plasma. Introductory, vol 1. Nauka, Moscow
48. Tinck S, Boullart W, Bogaerts A (2011) Modeling Cl₂/O₂/Ar inductively coupled plasmas used for silicon etching: effects of SiO₂ chamber wall coating. *Plasma Sources Sci Technol* 20:045012
49. Kuznetsova LA, Kuzmenko NE, Kuzyakov Yu Ya, Plastinin Yu A (1980) Transition probabilities of diatomic molecules. In: Khokhlov RV (ed) Moscow: Nauka
50. Radtsig AA, Smirnov BM (1978) Hand-book on atomic and molecular physics. Atomizdat, Moscow
51. Hagelaar GJM, Pitchford LC (2005) Solving the Boltzmann equation in the two-term approximation to obtain electron transport coefficients and rate coefficients for fluid models. *Plasma Sources Sci Technol* 14:722–733
52. Brotton SJ, McConkey JW (2011) Electron-impact dissociative excitation of S₂. *J Phys B: At Mol Opt Phys* 44:215202
53. Yamabe C, Buckman SJ, Phelps AV (1983) Measurement of free-free emission from low-energy-electron collisions with Ar. *Phys Rev A* 27:1345–1352
54. Brown PN, Byrne GD, Hindmarsh AC (1989) VODE: a variable-coefficient ODE solver. *SIAM J. Sci. Stat. Comput* 10(5):1038–1051
55. Lieberman MA, Lichtenberg AJ (1994) Principles of plasma discharges and materials processing. Wiley, New York